

Silver-Promoted High-Performance (Ag,Cu)(In,Ga)Se₂ Thin-Film Solar Cells Grown at Very Low Temperature

Shih-Chi Yang,* Jordi Sastre, Maximilian Krause, Xiaoxiao Sun, Ramis Hertwig, Mario Ochoa, Ayodhya N. Tiwari, and Romain Carron

Achieving high power conversion efficiencies with Cu(In,Ga)Se₂ (CIGS) solar cells grown at low temperature is challenging because of insufficient thermal energy for grain growth and defect annihilation, resulting in poor crystallinity, higher defect concentration, and degraded device performance. Herein, the possibilities for high-performing devices produced at very low temperatures (≤ 450 °C) are explored. By alloying CIGS with Ag by the precursor layer method, (Ag,Cu)(In,Ga)Se₂ (ACIGS) solar cells grown at about 450 °C reach an efficiency of 20.1%. Only a small efficiency degradation (0.5% and 1.6% absolute) is observed for ACIGS absorbers deposited at 60 and 110 °C lower substrate temperature. CIGS devices exhibit a stronger efficiency degradation, driven by a decrease in the open-circuit voltage (V_{OC}). The root cause of the V_{OC} difference between ACIGS and CIGS devices is investigated by advanced characterization techniques, which show improved morphology, reduced tail states, and higher doping density in ACIGS absorbers. The proposed approach offers several benefits in view of depositions on temperature-sensitive substrates. Increased Cu diffusion promoted by Ag allows end-point detection in the three-stage process at the substrate temperatures below 300 °C. The modified process requires minimal modification of existing processes and equipment and shows the potential for the use of different flexible substrates and device architectures.


research and investigations. Typically, a substrate temperature of ≥ 450 °C or higher is needed to obtain high efficiencies in CIGS solar cells. High substrate temperature hinders the use of many types of flexible substrates because of their thermal stability, such that polyimide (PI) is the substrate of choice owing to its compatibility to a temperature of up to about 450 °C. For instance, bifacial flexible CIGS solar cells could benefit from transparent substrates with low yellow index, e.g., colorless PI, but these are commonly only compatible with a substrate temperature lower than 350 °C. In addition, very low temperature processes offer additional advantages, such as a reduction of manufacturing costs and reduced thermal-induced stress. Nevertheless, the best performances of CIGS solar cells grown at very low temperatures (< 400 °C) with the common three-stage process are so far not competitive (18.0% at 390 °C^[3] and 12.4% at 350 °C^[4]). It is mainly because thermal energy is needed for Cu diffusion, as well as to promote grain growth and annihilate defects.^[4–6] Although single-stage low-

1. Introduction

Thin-film solar cells based on polycrystalline Cu(In,Ga)Se₂ (CIGS) have reached the efficiencies of 23.35%^[1] on glass and 20.8%^[2] on flexible substrates because of years of intensive

temperature pulsed electron deposition (LTPED) can yield the efficiencies up to 17.0% at 250 °C,^[7,8] this technique presents scale-up challenges and technical issues such as the presence of micrometer-sized particle.^[9] A simpler method offering high performance and a better potential for transferring from laboratory to manufacturing is, therefore, needed.

S.-C. Yang, J. Sastre, M. Krause, Dr. X. Sun, R. Hertwig, Dr. M. Ochoa, Prof. A. N. Tiwari, Dr. R. Carron
Laboratory for Thin Films and Photovoltaics
Empa - Swiss Federal Laboratories for Materials Science and Technology
Überlandstrasse 129, 8600 Dübendorf, Switzerland
E-mail: shih-chi.yang@empa.ch

 The ORCID identification number(s) for the author(s) of this article can be found under <https://doi.org/10.1002/solr.202100108>.

© 2021 The Authors. Solar RRL published by Wiley-VCH GmbH. This is an open access article under the terms of the Creative Commons Attribution-NonCommercial-NoDerivs License, which permits use and distribution in any medium, provided the original work is properly cited, the use is non-commercial and no modifications or adaptations are made.

Correction added on 10 April 2021, after first online publication: The copyright line was changed.

DOI: 10.1002/solr.202100108

(Ag,Cu)(In,Ga)Se₂ (ACIGS) has shown improved material properties as compared with CIGS, such as larger grain sizes,^[10] less structural defects, and less sub-bandgap disorder,^[11] which are connected to a lower melting point^[12] and enhanced elemental interdiffusion.^[13] The resulting high V_{OC} has drawn a lot of attention because of the potential for high-efficiency ACIGS solar cells.^[14–16] Furthermore, low-temperature grown ACIGS solar cells show comparable device performance with high-temperature grown CIGS solar cells,^[10] showcasing the possibility of further reduction of ACIGS absorber deposition temperature. However, most studies so far have focused on high deposition temperatures, and the lower bounds for processing temperatures have not been investigated yet.

Herein, we take advantage of the aforementioned properties of ACIGS to explore the processing temperature limits for high-performance ACIGS solar cells. We choose the Ag

precursor layer method^[13,17] for its simplicity and potential for easy implementation into existing CIGS co-evaporation equipment in research laboratories and industry. We modify the nominal substrate temperature (T_{sub}) of (A)CIGS absorbers in a wide range (from 413 to 253 °C), which is measured by thermocouple, to assess the beneficial effects from Ag. The upper nominal T_{sub} of 413 °C in this study corresponds to about 450 °C actual substrate temperature (about 37 °C difference). For T_{sub} below 413 °C, we expect a slightly smaller difference between T_{sub} and the actually substrate temperature. The changes in the solar cell performances are discussed in relation to changes in morphology, and the optoelectronic properties of the absorbers are investigated by scanning electron microscope (SEM), external quantum efficiency (EQE), Urbach tails, and time-resolved photoluminescence (TRPL).

2. Results and Discussion

Figure 1a–d summarizes the current–voltage (J – V) parameters of (A)CIGS solar cells with absorbers grown at different values of T_{sub} . The efficiency of CIGS solar cells decreases progressively and drops significantly for $T_{\text{sub}} < 353$ °C, mainly because of the reduced V_{OC} and to a lesser extent due to reduced fill factor (FF). On the contrary, the efficiency of ACIGS solar cells remains above 18.5% for T_{sub} above 303 °C, which is mainly driven by a lesser V_{OC} degradation as compared with CIGS solar cells. Furthermore, we see no clear downward trend in FF and J_{SC} for T_{sub} down to at least 303 °C in ACIGS. A distinct drop in both V_{OC} and FF is observed for ACIGS grown at 253 °C, resulting in an evident decrease in efficiency. To exclude the influence of E_g variations between different samples, we

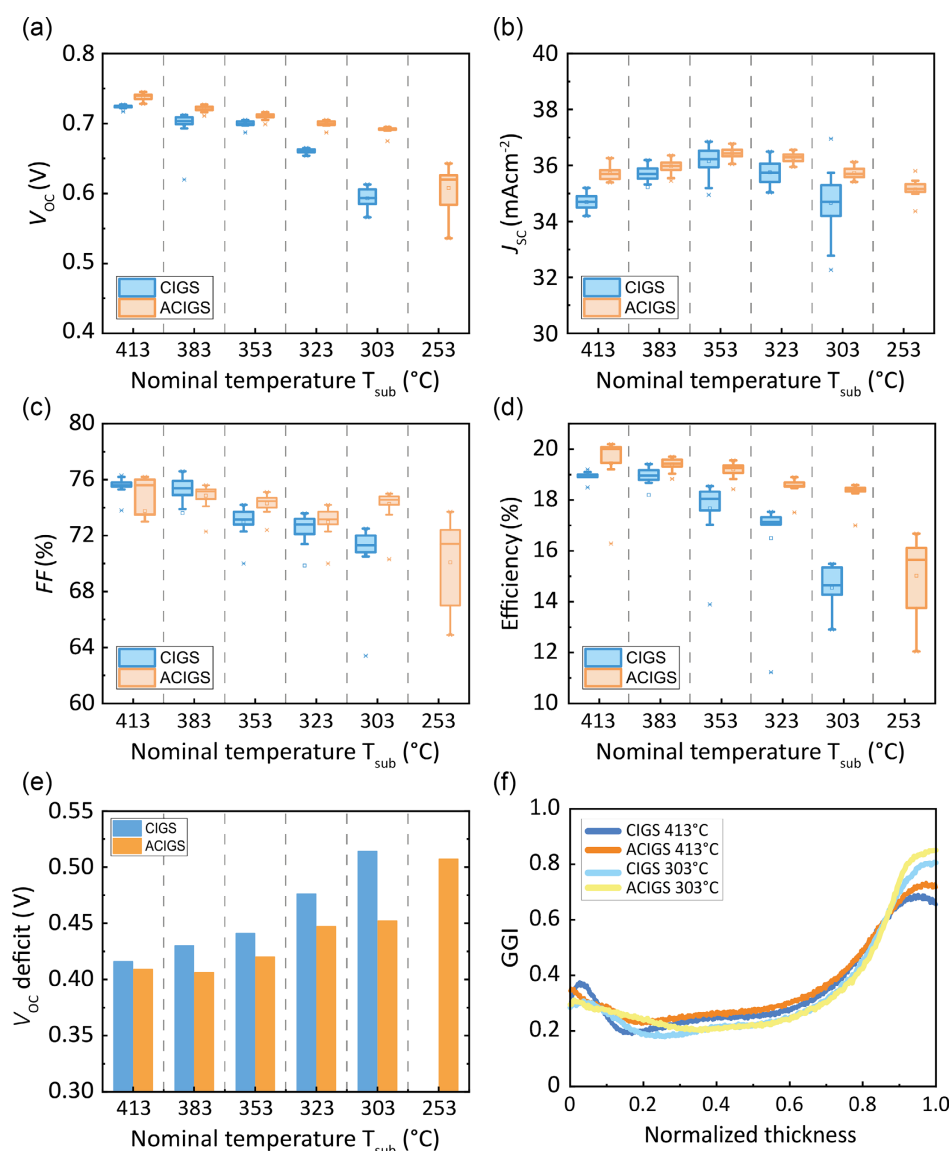


Figure 1. a–d) The J – V parameters of the (A)CIGS solar cells with varying nominal T_{sub} from 413 to 253 °C. e) $V_{\text{OC,def}}$ versus different nominal T_{sub} . $V_{\text{OC,def}}$ is calculated by $E_g/q - V_{\text{OC}}$, and the E_g values were determined by linear extrapolation of the plot $((\text{photon energy} \times \text{EQE})^2 \text{ vs photon energy})$ for values between 25% and 75% of the EQE maximum. f) GGI depth profiles for (A)CIGS absorbers grown at 413 and 303 °C.

further measured EQE (Figure S1, Supporting Information) and calculated the V_{OC} deficit, as shown in Figure 1e. For each T_{sub} investigated, ACIGS exhibits a lower $V_{OC,def}$ as compared with that of CIGS.

Time-of-flight secondary ion mass spectrometry (SIMS) measurements allow to assess the impact of Ag on the $[Ga]/([Ga] + [In])$ (GGI) grading. It has been reported that Ag reduces the GGI gradings significantly because of enhanced elemental interdiffusion.^[13] The GGI depth profiles in Figure 1f show a moderate influence of Ag on the back gradings. Ag also slightly flattens the notch region and modifies the front grading. The comparatively weaker influence of Ag on the GGI depth profiles may be related to the lower $[Ag]/([Ag] + [Cu])$ (AAC) of 4–5% (as compared with commonly used 20%^[14]) and the low T_{sub} ($\leq 450^\circ C$) used in our study. The SIMS measurements also reveal that Ag distribution is uniform for all the investigated T_{sub} (see Figure S2, Supporting Information).

To understand the reason for the low $V_{OC,def}$ in ACIGS, the microstructure of the ACIGS and CIGS absorbers was imaged by cross-sectional SEM (Figure 2a–e). We observe three main features of the absorber morphologies. First, the ACIGS layers present larger grain sizes for the same T_{sub} , as expected. Second, the typical small grain sizes found in the high GGI back region of CIGS are not observed in the ACIGS layers grown at $413^\circ C$. Ag improves the crystallinity even in the high Ga region. Finally, the ACIGS layer grown at $253^\circ C$ exhibits a larger grain size and a better morphology than the CIGS grown at higher T_{sub} of $303^\circ C$. Similar observations were previously reported between $580^\circ C$ grown ACIGS and $650^\circ C$ grown CIGS.^[10] Figure 2f shows the Urbach energy (E_U) estimated from the quasi-exponential decay in the long wavelength edge of the EQE curves. For the CIGS devices, E_U increases with lower T_{sub} , but for the ACIGS ones, E_U is almost independent from T_{sub} . Also, the E_U values of the ACIGS devices are always below or similar

to these of CIGS, suggesting a lesser density of structural and electronic defects.

The CIGS solar cells and layers deposited at $253^\circ C$ are missing because of the failure of the three-stage process. Specifically, the increase in the substrate heating regulation signal corresponding to the stoichiometric point was not able to be detected for CIGS grown at $253^\circ C$, as shown in Figure S3a,b, Supporting Information. A similar behavior was already reported before.^[4] This is because the Cu diffusion rate decreases: at low temperatures, Cu accumulates on the surface as a Cu–Se phase even before the stoichiometric point and is not available for the formation and recrystallization of the chalcopyrite phase. The accumulation of the Cu–Se phase on the surface can also explain the small increase in power output at around 32 min for the CIGS layer grown at $253^\circ C$ in Figure S3b, Supporting Information. On the contrary, the increase in power output is observed at around 47 min in the case of ACIGS grown at $253^\circ C$, and the layer underwent recrystallization. By adding Ag, the Cu diffusion rate is increased, extending the lower bound for process temperature. This lower bound of process temperature relates to the kinetics of Cu diffusion.^[5] By increasing Cu diffusion kinetics in the layers, the presence of Ag may help fast industrial processes to achieve complete layer recrystallization with minimized Cu excess requirement.

We performed TRPL to get insights into the electronic properties and carrier dynamics in the (A)CIGS absorbers. Figure 3a displays the selected TRPL decays from different absorbers. The decays were fitted with a two-exponential formula ($Y = A_1 \exp(-\frac{t}{\tau_1}) + A_2 \exp(-\frac{t}{\tau_2})$). Figure 3b,c shows the sum of the prefactors ($A = A_1 + A_2$) and the effective lifetime τ_{eff} calculated as $\tau_{eff} = \frac{A_1\tau_1 + A_2\tau_2}{A_1 + A_2}$ for the absorbers. As shown in Figure 3a, no fast initial decay is observed at early times, such that the sum of prefactors displayed in Figure 3b can be assumed proportional to the doping concentration in the absorbers. Above

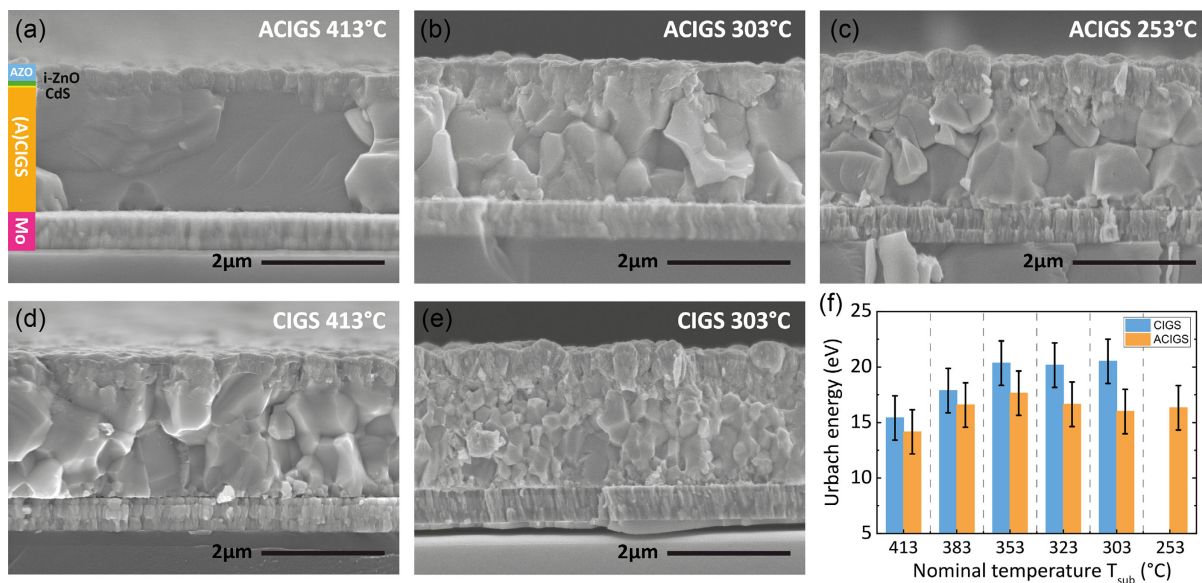


Figure 2. a–c) SEM cross-sectional images for ACIGS absorbers grown at nominal T_{sub} of 413, 303, and $253^\circ C$. d,e) SEM cross-sectional images for CIGS absorbers grown at nominal T_{sub} of 413 and $303^\circ C$. f) Urbach energy (E_U) of (A)CIGS versus different nominal T_{sub} .

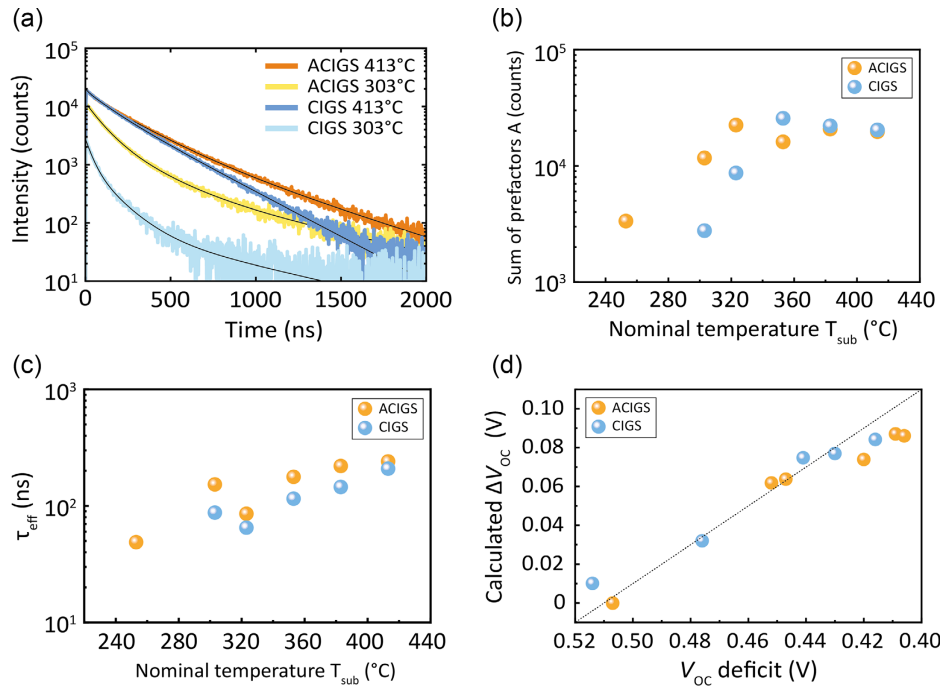


Figure 3. a) TRPL decays for (A)CIGS layers grown at 413 and 303 °C. b) Sum of prefactors $A_1 + A_2$ (A) of TRPL decays as a function of nominal T_{sub} . c) τ_{eff} of TRPL decays as a function of nominal T_{sub} . d) Relationship between ΔV_{OC} calculated from Equation (2) and the device $V_{OC,def}$.

353 °C, A for ACIGS absorbers is slightly lower than for CIGS, which is consistent with the reduced carrier concentration in ACIGS reported by other groups.^[13,18] However, CIGS experiences a significant drop in A below 353 °C, even lower than the values of ACIGS. In contrast, A drops for ACIGS only with the T_{sub} values below 303 °C. Similar trends are also found in the apparent doping concentration estimated from capacitance–voltage (C–V) measurements (Figure S4, Supporting Information). The τ_{eff} values of ACIGS layers are slightly higher than those of CIGS for all T_{sub} , which we attribute to the improved morphology, reduced density of grain boundaries, and to the lesser density of structural and electronic defects discussed earlier.

Following detailed balance principle, V_{OC} of (A)CIGS solar cells can be related to the external light emitting diode quantum efficiency (EQE_{LED}), as described by Equation (1),^[19] where V_{OC}^{rad} is the V_{OC} in the radiative limit and $-\frac{kT}{q} \ln(EQE_{LED})$ is associated with the nonradiative voltage losses. Ideally, the TRPL parameters τ_{eff} and A can be connected to EQE_{LED} . Hence, it is possible to calculate the relative difference in V_{OC} losses (ΔV_{OC}) for different samples by their ratio of EQE_{LED} , approached by their ratio of $A_1 \tau_1 + A_2 \tau_2$ (Equation (2)).

$$V_{OC,def}^{non-rad} = V_{OC}^{rad} - V_{OC} = -\frac{kT}{q} \ln(EQE_{LED}) \quad (1)$$

$$\begin{aligned} \Delta V_{OC} &= V_{OC,def}^{non-rad}_{ref} - V_{OC,def}^{non-rad}_{sample} = \frac{kT}{q} \ln\left(\frac{EQE_{LED,sample}}{EQE_{LED,ref}}\right) \\ &= \frac{kT}{q} \ln\left(\frac{(A_1 \tau_1 + A_2 \tau_2)_{sample}}{(A_1 \tau_1 + A_2 \tau_2)_{ref}}\right) \end{aligned} \quad (2)$$

The ACIGS absorber grown at 253 °C was chosen as the reference providing a ΔV_{OC} of 0 mV. Figure 3d compares the calculated ΔV_{OC} with the device $V_{OC,def}$. The data points closely follow the dashed line with slope of unity representing the expected behavior. TRPL data are a good predictor of the device $V_{OC,def}$. At higher T_{sub} , the high V_{OC} of ACIGS layers stems from longer τ_{eff} values. In contrast, low doping reduces V_{OC} of (A)CIGS solar cells grown at low T_{sub} . Ag extends the threshold T_{sub} at which doping starts to drop significantly, widening the T_{sub} process window for ACIGS by about 50 °C.

The residual stress in the absorbers is also an important parameter because of possible failure issues such as cracking, buckling, and delamination, especially for flexible applications. An X-ray diffraction (XRD) residual stress analysis^[20] was performed on the ACIGS and CIGS absorbers. The analysis was carried out on the (112) reflection measured with different ψ angles, defined as the angle between the scattering vector and the sample's normal direction. The residual stress in the films is calculated from the magnitude and direction of the peak shifts. **Figure 4a** summarizes the residual stress in absorbers grown at different values of T_{sub} . Both ACIGS and CIGS absorbers have compressive stress rather than tensile stress, in agreement with what was reported before for CIGS absorbers.^[5,21] Ag alloying significantly reduces the compressive stress (by about 50% for most of T_{sub} sample pairs). Figure 4b,c shows how the (112) peak of ACIGS and CIGS absorbers grown at 303 °C shifts as a function of the ψ angles. Peaks of both samples shift to the right with increasing ψ (compressive stress), but the shift is smaller for ACIGS than for CIGS. Our hypothesis for this behavior is that Ag helps to release the residual stress by enhanced elemental diffusion and grain growth. This makes ACIGS even more

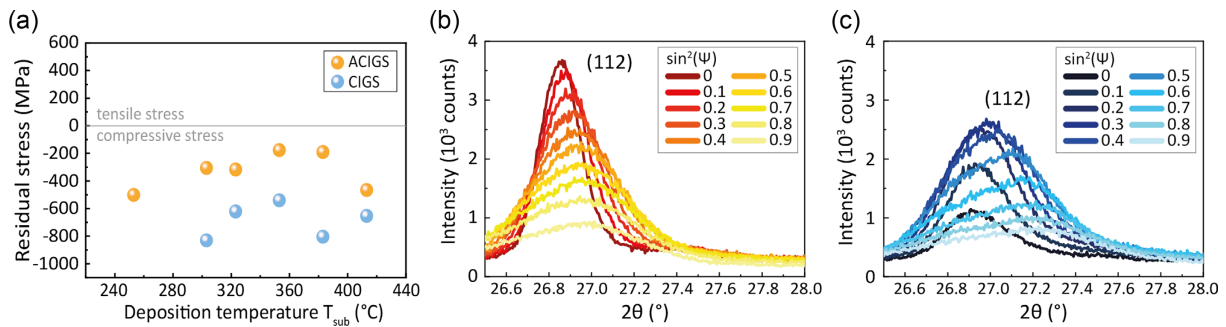


Figure 4. a) Residual stress as a function of nominal T_{sub} . b) (112) peak shift with various ψ angles for ACIGS grown at a nominal T_{sub} of 303 °C. c) (112) peak shift for CIGS grown at a nominal T_{sub} of 303 °C.

promising for a variety of flexible photovoltaics (PV) applications, for which adhesion issues are critical. It is worth mentioning that the residual stress shown in Figure 4a can be slightly underestimated because of the GGI gradings. The X-ray penetration depth is shallower at larger ψ angles. Thus, the diffraction angle of the (112) reflection may slightly shift toward lower values as a result of the increased sensitivity to the front region with larger lattice constant and smaller GGI. Nevertheless, a qualitative comparison of the residual stress between CIGS and ACIGS grown at the same T_{sub} is still valid, because CIGS and ACIGS have quite similar GGI gradings, as shown in Figure 1f, and are, therefore, similarly affected.

3. Conclusion

In summary, we successfully fabricated solar cells with CIGS and ACIGS absorbers deposited at very low T_{sub} from 413 down to 253 °C. As compared with regular CIGS, Ag alloyed absorbers displayed a number of advantageous characteristics summarized as follows. ACIGS devices outperformed CIGS ones, and high efficiencies were maintained over a wider temperature range: the efficiencies of 19.6% and 18.5% were achieved with a T_{sub} of 353 and 303 °C, respectively. J_{SC} remains essentially constant, and while FF plays a role, the loss of efficiency at very low temperature is mostly driven by V_{OC} degradation. ACIGS maintains high V_{OC} with substantially lower deposition temperatures than that of CIGS. Ag alloying improved the morphology of the absorbers and avoided too deteriorated morphology, which is obtained for low-temperature grown CIGS. The presence of Ag also reduces the density of structural and electronic defects as evidenced by E_{J} . Furthermore, the analysis of TRPL data detailed the causes for changes in $V_{\text{OC,def}}$ and discriminated two T_{sub} regimes. For CIGS, with T_{sub} above 350 °C, the moderate $V_{\text{OC,def}}$ degradation is driven by nonradiative recombination reflected by the τ_{eff} value. For T_{sub} below 350 °C, the strong performance degradation is mainly driven by the decrease in doping density. The threshold between the two regimes is lower by about 50 °C in the presence of Ag. Finally, ACIGS absorbers also present less residual stress than CIGS ones, which is advantageous in view of flexible PV applications. Our results suggest several superior properties of Ag alloying in industrial environment. The chosen Ag precursor layer method facilitates implementation into existing equipment in both industry and

research laboratories. The widened parameter window for substrate temperature relaxes manufacturing constraints and may contribute to reducing the manufacturing costs. The improved Cu diffusion in the presence of Ag also hints that deposition rates may be increased, and that the requirements on the Cu excess at the end of the second stage may be relaxed while ensuring complete layer recrystallization in fast industrial deposition processes.

4. Experimental Section

Soda-lime glass substrates were coated with a SiO_x barrier layer to prevent uncontrolled diffusion of alkali elements from the substrates, and with a Mo back contact (≈ 500 nm thick). For ACIGS absorbers, a 15 nm Ag layer was deposited by thermal evaporation on the Mo back contact before absorber deposition. The (A)CIGS absorbers were grown by a co-evaporation method with a multistage low-temperature deposition process as described in the previous study.^[22] Different nominal deposition temperatures were set for the second and third stages, ranging from 413 °C (compatible with PI substrates) down to 253 °C. The actual T_{sub} is about 30–50 °C higher than nominal temperature. After deposition, the absorbers were sequentially treated in situ with sodium fluoride (NaF) and rubidium fluoride (RbF) post-deposition treatments (PDT) of 20 min each in Se ambient. The integrated GGI and [Cu]/([Ga] + [In]) (CGI) values of CIGS absorbers were determined by X-ray fluorescence (XRF), previously calibrated with a reference. The cells were completed with a 30 nm cadmium sulfide (CdS) buffer layer by chemical bath deposition, a radio-frequency-sputtered window consisting of an 80 nm intrinsic zinc oxide (ZnO) and a 200 nm Al-doped (Al_2O_3 2 wt%) ZnO, electron beam evaporated Ni/Al grids, and a MgF_2 antireflective coating. Cells of ≈ 0.57 cm² area were defined by mechanical scribing.

J - V parameters were measured using a four-terminal Keithley 2400 source meter under standard test conditions (25 °C, 1000 Wm^{-2} , AM1.5G illumination, ABA-class sun simulator). EQE was measured using a chopped illumination from a halogen light source, wavelength-selected with a double-grating monochromator. A halogen lamp light bias of about 0.2 sun intensity was applied during the measurements. A certified Si and a calibrated Ge solar cells were used for calibration. C - V profiles were measured with an Agilent E4980A LCR meter at a frequency of 1 kHz and a temperature of 300 K. Carrier concentrations were extracted from the apparent doping curve at an applied voltage of zero assuming an n^+ p junction. Compositional depth profiles were measured by SIMS. The primary beam was 25 keV Bi^+ with a total current of 0.6 pA and a raster size of 50×50 μm^2 . The sputtering beam was 250 nA, 2 keV O^{2+} with an on-sample area of 300×300 μm^2 . GGI depth profiles were determined by scaling the elemental traces with integral GGI values obtained from XRF. TRPL measurements were performed using a 639 nm diode laser with 100 ps pulse duration as excitation source, and an InGaAs

photomultiplier in combination with a PicoQuant time correlated single-photon counting electronics for signal acquisition. The pulse repetition rates were 0.3 MHz. The illumination spot size was around 130 μm diameter. The corresponding photon density was around $3 \times 10^{11} \text{ cm}^{-2}$ per pulse. Before TRPL measurements, the window layers were etched away in acetic acid, leaving a thin CdS layer on the absorber. Cross-sectional images were acquired using a Hitachi S-4800 SEM. The XRD residual stress analysis was performed in a Bruker D8 Discover XRD system with $\text{CuK}\alpha_1$ radiation.

Supporting Information

Supporting Information is available from the Wiley Online Library or from the author.

Acknowledgements

This work received funding from the Swiss Federal Office of Energy (SFOE) under ImproCIS project (Contract no.: SI/501614-01) and from the Swiss State Secretary for Education, Research and Innovation (SERI) under contract number 17.00105 (EMPIR project HyMet). The EMPIR programme is co-financed by the participating States and by the European Union's Horizon 2020 research and innovation programme under grant agreement No 850937. X.S. acknowledges funding from the ETH Zurich Postdoctoral Fellowship. M.K. acknowledges funding from the European Union's Horizon 2020 research and innovation programme under grant agreement No 850937. J.S. acknowledges funding from the Swiss National Science Foundation (grant number 200021_172764).

Conflict of Interest

The authors declare no conflict of interest.

Data Availability Statement

The data that support the findings of this study are available from the corresponding author upon reasonable request.

Keywords

Ag alloying, (Ag,Cu)(In,Ga)Se₂, Cu(In,Ga)Se₂, interdiffusion, low substrate temperatures, V_{OC} deficit

Received: February 8, 2021

Revised: February 25, 2021

Published online: March 19, 2021

- [1] M. Nakamura, K. Yamaguchi, Y. Kimoto, Y. Yasaki, T. Kato, H. Sugimoto, *IEEE J. Photovoltaics* **2019**, *9*, 1863.
- [2] R. Carron, S. Nishiwaki, T. Feurer, R. Hertwig, E. Avancini, J. Löckinger, S.-C. Yang, S. Buecheler, A. N. Tiwari, *Adv. Mater. (Weinheim, Ger.)* **2019**, *9*, 1900408.
- [3] M. Balestrieri, V. Achard, T. Hildebrandt, L. Lombez, M. Jubault, J. Posada, D. Lincot, F. Donsanti, *J. Alloys Compd.* **2019**, *794*, 654.
- [4] S. Nishiwaki, T. Satoh, Y. Hashimoto, T. Negami, T. Wada, *J. Mater. Res.* **2001**, *16*, 394.
- [5] R. Mainz, H. Rodriguez-Alvarez, M. Klaus, D. Thomas, J. Lauche, A. Weber, M. Heinemann, S. Brunken, D. Greiner, C. Kaufmann, T. Unold, H.-W. Schock, C. Genzel, *Phys. Rev. B* **2015**, *92*, 155310.
- [6] L. Zhang, Q. He, W.-L. Jiang, F.-F. Liu, C.-J. Li, Y. Sun, *Sol. Energy Mater. Sol. Cells* **2009**, *93*, 114.
- [7] M. Mazzer, S. Rampino, E. Gombia, M. Bronzoni, F. Bissoli, F. Pattini, M. Calicchio, A. Kingma, F. Annoni, D. Calestani, N. Cavallari, V. T. Vijayan, M. Lomascolo, A. Creti, E. Gilioli, *Energies* **2016**, *9*, 207.
- [8] M. Mazzer, S. Rampino, G. Spaggiari, F. Annoni, D. Bersani, F. Bissoli, M. Bronzoni, M. Calicchio, E. Gombia, A. Kingma, F. Pattini, E. Gilioli, *Sol. Energy Mater. Sol. Cells* **2017**, *166*, 247.
- [9] P. Kuppusami, V. Raghunathan, *Surf. Eng.*, **2006**, *22*, 81.
- [10] L. Chen, J. Lee, W. N. Shafarman, *IEEE J. Photovolt.* **2013**, *4*, 447.
- [11] P. T. Erslev, J. Lee, G. M. Hanket, W. N. Shafarman, J. D. Cohen, *Thin Solid Films* **2011**, *519*, 7296.
- [12] G. M. Hanket, J. H. Boyle, W. N. Shafarman, in *2009 34th IEEE Photovoltaic Specialists Conference (PVSC)*, IEEE, Piscataway, NJ **2009**, pp. 1240–1245.
- [13] G. Kim, W. M. Kim, J.-K. Park, D. Kim, H. Yu, J.-H. Jeong, *ACS Appl. Mater. Interfaces* **2019**, *11*, 31923.
- [14] M. Edoff, T. Jarmar, N. S. Nilsson, E. Wallin, D. Högström, O. Stolt, O. Lundberg, W. Shafarman, L. Stolt, *IEEE J. Photovolt.* **2017**, *7*, 1789.
- [15] Y. Zhao, S. Yuan, D. Kou, Z. Zhou, X. Wang, H. Xiao, Y. Deng, C. Cui, Q. Chang, S. Wu, *ACS Appl. Mater. Interfaces* **2020**, *12*, 12717.
- [16] MiaSolé, Press release, **2019**, <http://miasole.com/miasole-achieves-flexible-substrate-thin-film-solar-cell-efficiency-of-20-56-percent/> (accessed: July 2019).
- [17] K. Kim, J. W. Park, J. S. Yoo, J.-S. Cho, H.-D. Lee, J. H. Yun, *Sol. Energy Mater. Sol. Cells* **2016**, *146*, 114.
- [18] N. Valdes, J. Lee, W. Shafarman, *Sol. Energy Mater. Sol. Cells* **2019**, *195*, 155.
- [19] U. Rau, *Phys. Rev. B* **2007**, *76*, 085303.
- [20] S. Malhotra, Z. Rek, S. Yalisove, J. Bilello, *Thin Solid Films* **1997**, *301*, 45.
- [21] Y.-C. Lin, X.-Y. Peng, L.-C. Wang, Y.-L. Lin, C.-H. Wu, S.-C. Liang, *J. Mater. Sci.: Mater. Electron.* **2014**, *25*, 461.
- [22] E. Avancini, R. Carron, B. Bissig, P. Reinhard, R. Menozzi, G. Sozzi, S. D. Napoli, T. Feurer, S. Nishiwaki, S. Buecheler, A. N. Tiwari, *Prog. Photovoltaics Res. Appl.* **2017**, *25*, 233.